https://doi.org/10.5194/wes-2026-205
Preprint. Discussion started: 4 November 2026
© Author(s) 2026. CC BY 4.0 License.



eawe european academy of wind energy
Open Access WIND ENERGY SCIENCE DISCUSSIONS

Pitch Control Applied to Troposkein-shaped Darrieus Vertical Axis Wind Turbines: Power and Loads Impacts

Daniel Bouzolin[1] and D. Todd Griffith[1]

[1]UTD Center for Wind Energy, Department of Mechanical Engineering, University of Texas at Dallas, Richardson, Texas, USA

Correspondence: D. Todd Griffith (tgriffith@utdallas.edu)

Abstract. The present study investigates the novel application of pitch control to a troposkein-shaped Darrieus vertical axis wind turbine (VAWT). Despite the widespread usage of pitch control in horizontal axis wind turbines and straight-bladed H-type VAWTs, pitch control has never been implemented in a troposkein-shaped Darrieus VAWT due to its prohibitively complex curved blade geometry. In this work, a stall-regulated Darrieus VAWT is converted to a pitch-controlled design using partial-span blade and strut pitching. The performance of the pitch-controlled rotor is analyzed using a free-wake vortex code (CACTUS) and compared to that of the stall-regulated design. Results indicate that pitching only a partial blade span and/or struts enables the regulation of rated power in a Darrieus VAWT. Further, this new application of pitch control in troposkein-shaped Darrieus VAWTs provides a significant increase in annual energy production (AEP) and significant reduction of fatigue loads (i.e., damage equivalent loads) for thrust, lateral, and torque loads. However, these improvements come at the cost of increased peak thrust loads. The findings of this study lay the foundation for promising new operating strategies using partial span blade pitch and/or strut pitch control for troposkein-shaped Darrieus VAWTs.

1 Introduction

The vertical axis wind turbine (VAWT) has long been thought of as less efficient than its more traditional and widespread counterpart, the horizontal axis wind turbine (HAWT). However, most VAWT studies have focused on small-scale, low-Reynolds-number designs, whereas there is a clear increase in the power coefficient (C_P) with increasing Reynolds numbers (Bourhis et al., 2023; Miller et al., 2018) in megawatt-scale rotors. Furthermore, some megawatt-scale VAWT designs rival and can even surpass the C_P of megawatt-scale HAWTs (Paraschivoiu et al., 2018). Vertical axis turbines have the added advantage of better wake recovery compared to HAWTs, leading to better overall wind farm performance (Brownstein et al., 2016; Bensason et al., 2025). Another important factor for power efficiency, however, is the use of active control strategies. Whereas active control is highly mature in HAWTs, active control strategies in VAWTs are less commonly studied and developed. To unlock the greatest efficiency gains in VAWTs, it is imperative that these strategies are researched and developed.

Much like in HAWTs, vertical axis turbine performance under pitch control (applied in prior studies only to H-type VAWTs) has many benefits compared to the performance of a stall-regulated scheme. Blade pitching in H-type VAWTs has primarily been used to improve aerodynamic efficiency (Region 2 operation) or maintain a desired power rating (Region 3 operation),

https://doi.org/10.5194/wes-2026-205
Preprint. Discussion started: 4 November 2026
© Author(s) 2026. CC BY 4.0 License.



eawe european academy of wind energy
Open Access WIND ENERGY SCIENCE DISCUSSIONS

though it can also be used to modulate loads on the rotor. A review of the literature indicates a broad spectrum of implementations and uses for blade pitching across a wide range of H-type VAWT designs, including enhanced power performance, load reductions, or wake steering behavior. A brief synopsis of these studies is presented here.

The idea of blade pitching for enhanced power performance in H-type (straight-bladed) VAWTs is not new: in the late 1970s, work was done in electrical actuation for blade "rocking" (pitching) that would maintain a constant angle of attack throughout the rotor revolution and maximize power capture (McConnell, 1979). In the 90s, Kirke and Lazauskas (1991) revisited the idea of electrical actuation for blade pitching and instead conceptualized a self-acting variable pitch system for an H-type VAWT, which was shown to improve both self-starting capability and power performance. More recently, Le Fouest and Mulleners (2024) experimentally sought an optimal blade pitch profile for enhancing power production or reducing load fluctuations in an H-type VAWT. Though they studied only one blade, they found several pareto-optimal individual pitch profiles which could either increase the power coefficient or decrease load fluctuations by delaying and mitigating deep dynamic stall. Ribeiro et al. (2024) investigated H-type VAWT wake steering through a collective pitching action of both blades and struts, finding that doing so creates highly favorable wake behavior and power availability for downstream turbines. Gupta et al. (2024) performed Computational Fluid Dynamics (CFD) simulations to study variable pitching in a two-dimensional H-type VAWT model. They obtained significant performance improvements by increasing blade pitch angles to stay within an optimal angle of attack range, produce maximum lift, and eliminate negative torque during cyclic operation. Rezaeiha et al. (2017) performed a similar CFD study, though they only considered fixed pitch angles for blade performance enhancement. Even with fixed blade pitch, they were able to slightly improve the coefficient of power, though larger pitch angles typically caused blade angle of attack to exceed the static stall angle.

Aside from blade pitch control, several alternative control strategies exist for Darrieus VAWTs. Some of these methods, much like blade pitch control, are mechanical in nature (e.g., Gurney flaps and trailing edge flaps). Bianchini et al. (2019) performed a CFD study to investigate the use of Gurney flaps for power enhancement of Darrieus VAWTs and found that the power coefficient could be increased up to 20 % at low-to-medium tip speed ratios. However, they also found the performance of a fixed flap configuration suffered at certain azimuthal angles and higher operating speeds due to larger drag penalties. To overcome this limitation, Zereg et al. (2024) performed a similar study but used oscillating Gurney flaps, yielding a 19 % increase in the mean torque coefficient at a TSR of 2.04. Other control methods involve active flow control, avoiding the need for moving parts entirely. Greenblatt et al. (2012) experimentally demonstrated the effectiveness of leading-edge dielectric barrier discharge (DBD) plasma actuators, improving gross turbine power production up to 38 %, though not necessarily maintaining net-positive energy gains (which were shown to be scale-dependent). More recently, Daraee and Abbasi (2023) numerically investigated an optimal strategy for DBD plasma actuators and achieved a 29.2 % increase in the turbine power coefficient and a 6.3 % net power gain after accounting for actuator power consumption. Jafari et al. (2022) experimentally investigated the use of not only plasma actuation, but also intracycle RPM control, which is a generator-based control strategy that requires no additional components at all. They found that plasma actuation was able to improve the experimentally measured power coefficient, particularly at lower wind speeds, and that intracycle RPM control was able to improve the average power coefficient up to 28 %. Sadman Sakib et al. (2023) applied an intracycle RPM control strategy to a 5 MW Darrieus VAWT, numerically

https://doi.org/10.5194/wes-2026-205
Preprint. Discussion started: 4 November 2026
© Author(s) 2026. CC BY 4.0 License.



eawe european academy of wind energy
Open Access WIND ENERGY SCIENCE DISCUSSIONS

demonstrating that annual energy production (AEP) of a 2-bladed turbine could be increased by 4.2 % without increasing loads, or up to 22.5 % with an increased load limit (1.2× baseline). Reeves and Griffith (2025) extended this work to evaluate broader system-level impacts, showing that modifying rotor inertia along with intracycle RPM control enhances energy capture and significantly reduces generator torque fatigue loads.

The main contribution from the present study arises from the extension of collective pitch control – a control strategy previously confined to HAWTs and H-type VAWTs – to troposkein-shaped Darrieus VAWTs. Traditionally, the highly curved troposkein-shaped blade shape has prohibited pitching of the blades. This limitation is overcome in the current study by analyzing partial blade span sections and horizontal struts as pitchable segments. The main findings of the study show that this application of pitch control in troposkein-shaped Darrieus VAWTs is capable of regulation of power in above-rated conditions. Further, this application of pitch control improves AEP significantly relative to a stall-regulated baseline case. In addition, the thrust, lateral, and torque damage-equivalent loads are greatly reduced relative to the stall-regulated baseline, although peak thrust loads increase relative to the baseline. Overall, these findings indicate that pitch control could play a pivotal role in the deployment of troposkein-shaped Darrieus VAWTs for the larger global transition to clean and efficient energy systems.

The remainder of this paper is organized as follows. Section 2 describes the methods used to set up simulations, quantify annual energy production, and compute damage equivalent loads. Section 3 illustrates the resulting impacts of pitch control on power and loads of the troposkein-shaped Darrieus VAWT. Section 4 discusses more details of the mechanisms driving these power and loads changes. Section 5 notes a few key conclusions and provides a brief outlook for future work.

2 Methods

2.1 VAWT Aerodynamics

The concept of using blade pitch to regulate power and loads in a VAWT rotor is motivated by the rotor's underlying aerodynamic principles. Though the Darrieus turbine is an inherently complex, three-dimensional structure, we may consider for a moment a simplified two-dimensional blade element to examine some of the key aerodynamic principles driving VAWT rotor loading.

VAWT blade aerodynamics (including lift and drag coefficients) are highly dependent upon the angle of attack of the airfoil section under consideration (Sakib and Griffith, 2022; De Tavernier et al., 2022). The angle of attack is the angle from the relative velocity vector V_{rel} (a combination of the freestream wind velocity u_∞, turbine rotational velocity ω, and rotor induced velocity) to the airfoil chordline (line from the leading edge to trailing edge). The angle of attack can be defined as follows:

$$\alpha = \psi + \beta \tag{1}$$

where the inflow angle ψ is the defined as the angle from the relative velocity vector to the tangent of the rotational path, and the pitch angle β is defined as the angle from the tangent of the rotational path to the airfoil chordline, as illustrated in Fig. 1. Note that the pitch angle directly affects the angle of attack experienced by the airfoil section, and thus can be used to modulate the lift, drag, and by extension, power and loads of the turbine.

https://doi.org/10.5194/wes-2026-205
Preprint. Discussion started: 4 November 2026
© Author(s) 2026. CC BY 4.0 License.

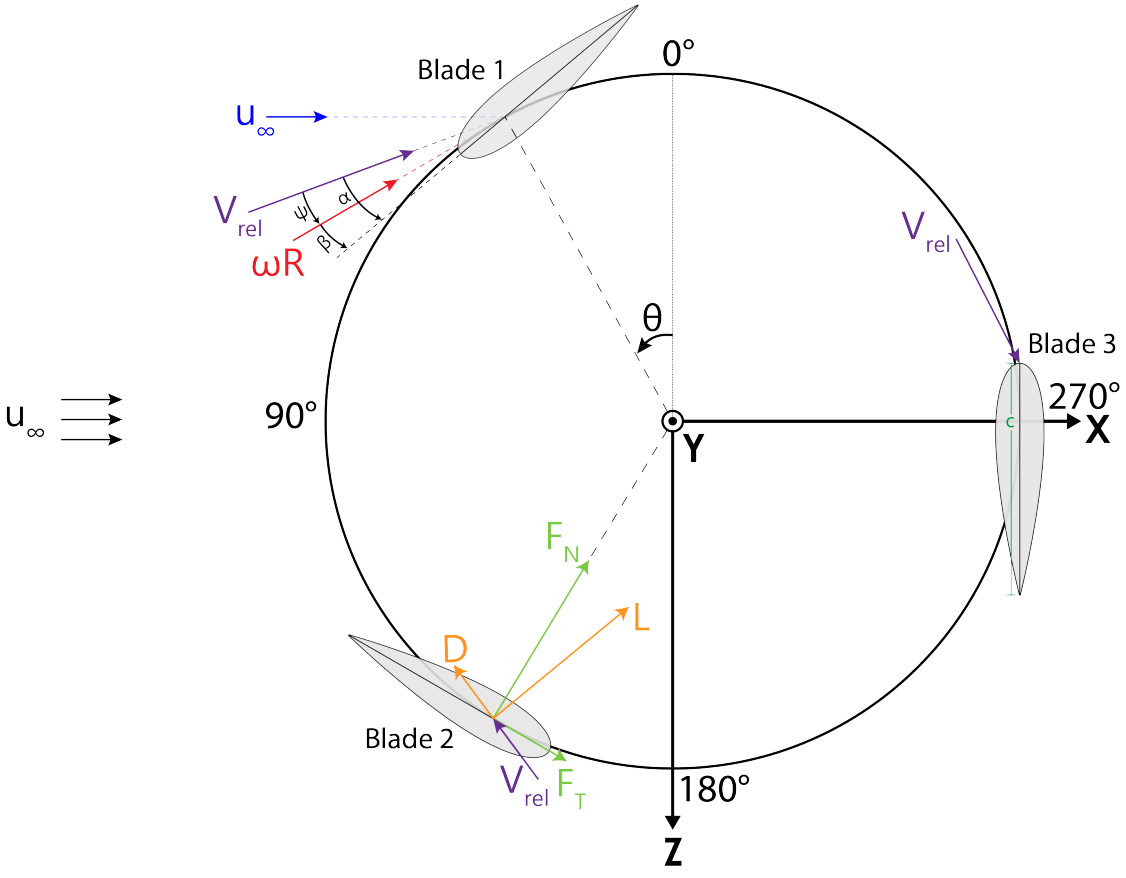


Figure 1. Two-dimensional VAWT airfoil section with aerodynamic forces shown. Blades 2 and 3 are unpitched, as shown. Blade 1 (at the 30° azimuthal location) is shown with a nonzero pitch angle $\beta = 10°$ to illustrate Equation (1).

The 2D lift and drag per unit span on an airfoil section are given by the following equations:

$$L = \frac{1}{2}\rho c V_{\text{rel}}^2 C_L(\alpha) \tag{2}$$

$$D = \frac{1}{2}\rho c V_{\text{rel}}^2 C_D(\alpha) \tag{3}$$

where ρ is the air density, c is the airfoil chord length, and the coefficients of lift and drag C_L and C_D are given as a function of the angle of attack of the airfoil. The normal and tangential forces on an airfoil section are dependent upon these forces, such that

$$F_N = L\cos(\psi) + D\sin(\psi) \tag{4}$$

$$F_T = L\sin(\psi) - D\cos(\psi) \tag{5}$$

https://doi.org/10.5194/wes-2026-205
Preprint. Discussion started: 4 November 2026
© Author(s) 2026. CC BY 4.0 License.



eawe european academy of wind energy
Open Access WIND ENERGY SCIENCE DISCUSSIONS

Thus, the lift and drag forces (and by extension, the normal and tangential forces on the rotor) show a clear dependence on the angle of attack. The power and thrust per unit span in a single revolution of the rotor can then be expressed by

$$P = \frac{B}{2\pi} \int_0^{2\pi} F_T(\theta) \cdot \omega R \, d\theta \tag{6}$$

$$T = \frac{B}{2\pi} \int_0^{2\pi} \left(F_N(\theta) \sin(\theta) - F_T(\theta) \cos(\theta) \right) d\theta \tag{7}$$

where B is the number of blades and θ is the rotor azimuth angle. From the equations above, two key relationships can be noted. First, rotor power and loading changes can be imparted through a change in V_{rel}. This means that a change in rotor speed ω will necessarily propagate to a change in rotor power and loads—not only by affecting the power equation $P = Q\omega$ (where Q is the rotor torque), but also by modifying the relative velocity that the lift and drag terms depend on. Second, rotor power and loading changes can be brought about by a change in pitch angle β. The angle of attack α is directly dependent upon the pitch angle (Eq. 1), which directly affects the lift and drag coefficients used in Eqs. (2)–(7). These relationships, along with the equations derived above, are further leveraged in Sect. 4 to explain the physical mechanisms driving the power and load changes observed under pitch control.

2.2 Model Definition

The VAWT model chosen for this study is a multi-megawatt troposkein-shaped Darrieus VAWT design, denoted here as the UTD 5MW design. Some key parameters of the model for the UTD 5MW design are shown in Table 1.

Table 1. Turbine parameters of the UTD 5MW Darrieus VAWT.

Parameter	Value	Unit
Airfoil Type	NACA 0021	–
Number of Blades	3	–
Blade Chord (root)	5.6	m
Blade Chord (equator)	2.8	m
Rotor Radius	54.01	m
Blade Length	177.8	m
Rotor Solidity	0.14	–
Rated Power	5	MW
Cut-in Wind Speed	5	$\mathrm{m\,s^{-1}}$
Rated Wind Speed	15	$\mathrm{m\,s^{-1}}$
Cut-out Wind Speed	25	$\mathrm{m\,s^{-1}}$

https://doi.org/10.5194/wes-2026-205
Preprint. Discussion started: 4 November 2026
© Author(s) 2026. CC BY 4.0 License.



eawe european academy of wind energy
Open Access WIND ENERGY SCIENCE DISCUSSIONS

115 According to Table 1, the blade chord differs at the root and equator. This is due to the blade tapering, which improves the power coefficient and structural performance of the blade while keeping blade mass increase manageable (Sakib and Griffith, 2022). Along the equatorial section of the blade, the chord is kept constant. The blade chord maintains this constant value from the equator until the strut mountpoints, after which it tapers linearly to the root chord value at the turbine tower. The strut mountpoints in this study were selected to be at 20 % along the tower height, as measured from top and bottom of the rotor, 120 which provided a pitchable blade section length of 43.59 m and a pitchable strut section length of 34.56 m.

To assess the trade-offs between aerodynamic control capability and mechanical complexity, four different collective pitching strategies are evaluated in this study. These include the stall-regulated baseline, partial-span blade-only pitching, strut-only pitching, and combined partial-span blade and strut pitching, as illustrated in Fig. 2. The primary focus of this study is on a 3-bladed rotor configuration, and thus all results will pertain to this rotor. However, an investigation of pitch control applied to 125 an aerodynamically equivalent 2-bladed rotor configuration is also conducted and detailed in Appendix B.

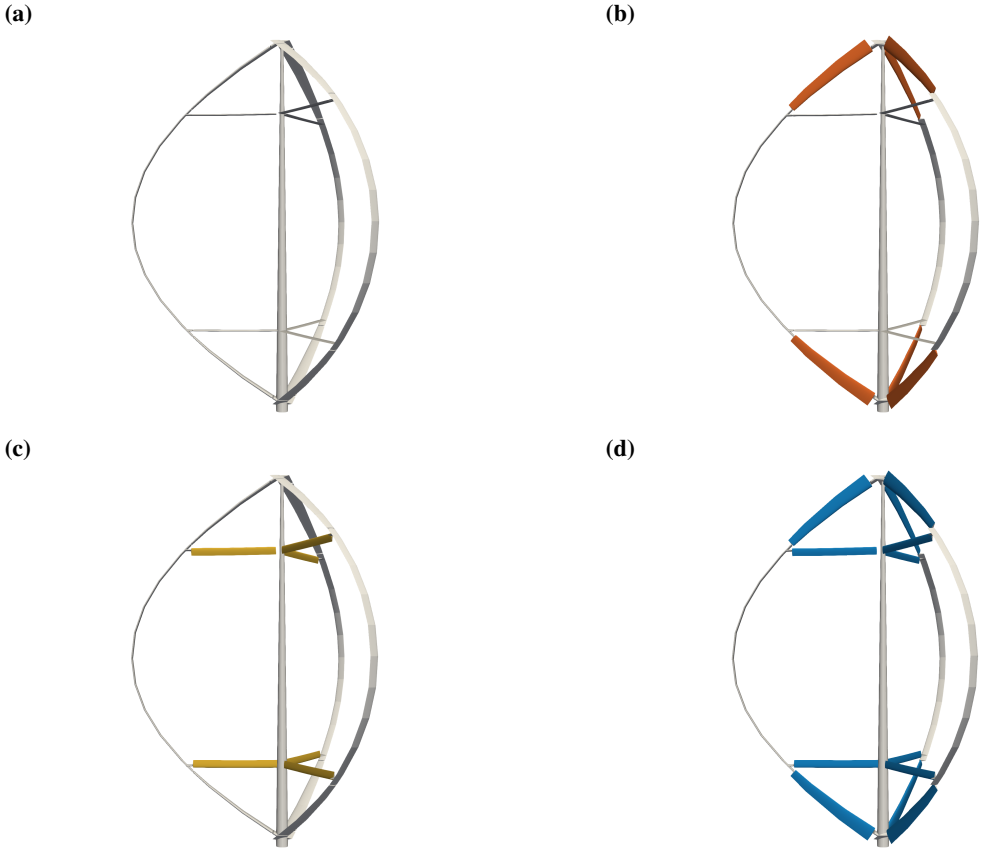


Figure 2. Illustration of four different rotor designs, each corresponding to a different operating strategy. Pitchable portions are highlighted to showcase (a) stall-regulated baseline, (b) partial-span blade-only pitching, (c) strut-only pitching, and (d) combined partial-span blade and strut pitching.

https://doi.org/10.5194/wes-2026-205
Preprint. Discussion started: 4 November 2026
© Author(s) 2026. CC BY 4.0 License.



eawe european academy of wind energy
Open Access WIND ENERGY SCIENCE DISCUSSIONS

2.3 Aerodynamic Simulation

2.3.1 Simulation Setup and Operating Strategy Development

This study used CACTUS (Code for Axial and Crossflow Turbine Simulation) to evaluate the performance of the stall-regulated and pitch-controlled designs. CACTUS is a mid-fidelity free-wake vortex code for turbine performance simulation that can simulate an arbitrary vertical axis turbine using a number of discretized lifting-line blade elements for each blade and free vortex line elements for the wake (Murray and Barone, 2011). Typically, CACTUS uses a simplified empirical model for calculating strut loads, and struts do not shed a free vortex wake. For the purposes of this study, however, the CACTUS model definition was modified to model all blades and struts as lifting-line blades. This enables the investigation of not only the blade-only pitching strategy, but also the strut-only and combined blade and strut pitching strategies as a means for pitch control.

Each of the four cases analyzed in this study is designed to have a baseline operating strategy—that is, to operate under a given RPM versus wind speed (and pitch angle versus wind speed) curve. The operating strategy for each rotor is developed using a two-step sequential methodology, as described below.

In the first step of operating strategy development, the rotor RPM schedule versus wind speed is established to track the optimal tip speed ratio ($\mathrm{TSR_{opt}}$) corresponding to the maximum power coefficient ($C_{p,\max}$) in Region 2 (below-rated operation), capping itself at a prescribed rated RPM limit. For the stall-regulated baseline, this rated limit is governed by the rotational speed required to passively stall the rotor at rated power (Sakib and Griffith, 2022). In essence, the RPM at each wind speed is taken as $\min[\mathrm{RPM_{opt}},\ \mathrm{RPM_{stall}}]$, where $\mathrm{RPM_{opt}}$ is the RPM corresponding to the optimal TSR for that wind speed, and $\mathrm{RPM_{stall}}$ is the RPM needed for the rotor to achieve rated power in stalled conditions at the prescribed rated wind speed ($15\,\mathrm{m\,s^{-1}}$ in this case). This causes the operating strategy to follow a linear RPM ramp-up in Region 2 operation, followed by a constant RPM in Region 3. More details on the development of the operating strategy for the stall-regulated rotor can be found in Sakib and Griffith (2022). For the pitch-controlled cases, RPM versus wind speed is determined in a similar way. However, the rotor RPM is now able to follow a linear ramp-up for a wider range of wind speeds. This means that the RPM is now selected as $\min[\mathrm{RPM_{opt}},\ \mathrm{RPM_{rated}}]$, where $\mathrm{RPM_{rated}}$ is the RPM that causes the rotor to generate the rated power of 5 MW at the rated wind speed (which now occurs at a lower wind speed due to the rotor operating at $C_{p,\max}$ for a wider range of wind speeds).

In the second step of operating strategy development, collective pitch angle schedules are designed for above-rated wind speeds (Region 3) to shed excess aerodynamic torque and regulate the rotor's power output to 5 MW. If the initial operating strategy led to an operating condition in which the rotor was not able to maintain 5 MW of rated power while keeping pitch actuation below 90° (which occurs only for the strut-only pitching case), then the optimizer enters a binary search to look for a new rated RPM limit. The new rated RPM limit is determined such that it enables the rotor to maximize its rated RPM and range of wind speeds for which it maintains $C_{p,\max}$ while keeping pitch actuation within the specified limit of 90°. The resulting rotational speed, tip speed ratio, power coefficient, and pitch angle schedules are evaluated in Sect. 3.1.

https://doi.org/10.5194/wes-2026-205
Preprint. Discussion started: 4 November 2026
© Author(s) 2026. CC BY 4.0 License.



eawe european academy of wind energy
Open Access WIND ENERGY SCIENCE DISCUSSIONS

2.3.2 Kinematic Formulation of Blade Pitching

Blade pitching in a troposkein-shaped Darrieus VAWT requires rotating each pitchable section about its local spanwise axis. This method of pitching the blades and struts was implemented in the CACTUS model geometry through the application of the Rodrigues' rotation formula. Rodrigues' rotation formula (Rodrigues, 1840), widely used for axis-angle coordinate transformations in kinematic systems (Murray et al., 1994), defines the rotation of any vector $\boldsymbol{v}$ about a unit axis $\hat{\boldsymbol{k}}$ by an angle β as follows:

$$\boldsymbol{v}_{\text{rot}} = \boldsymbol{v}\cos(\beta) + (\hat{\boldsymbol{k}} \times \boldsymbol{v})\sin(\beta) + \hat{\boldsymbol{k}}(\hat{\boldsymbol{k}} \cdot \boldsymbol{v})(1 - \cos(\beta)) \tag{8}$$

The CACTUS code defines blade geometry through a series of tangent and normal vectors at each node along the blade. These vectors are used to model the orientation of blade elements, including their associated pitch angle. Equation (8) is applied to the baseline, non-pitched blade elements to rotate the tangent vector about the unit local spanwise vector by an angle β, which results in the new (pitched) tangent vector as shown in Fig. 3. The cross product of the spanwise vector and this new tangent vector provides the definition for the new normal vector of the blade, which completes the definition of the pitched blade geometry in CACTUS.

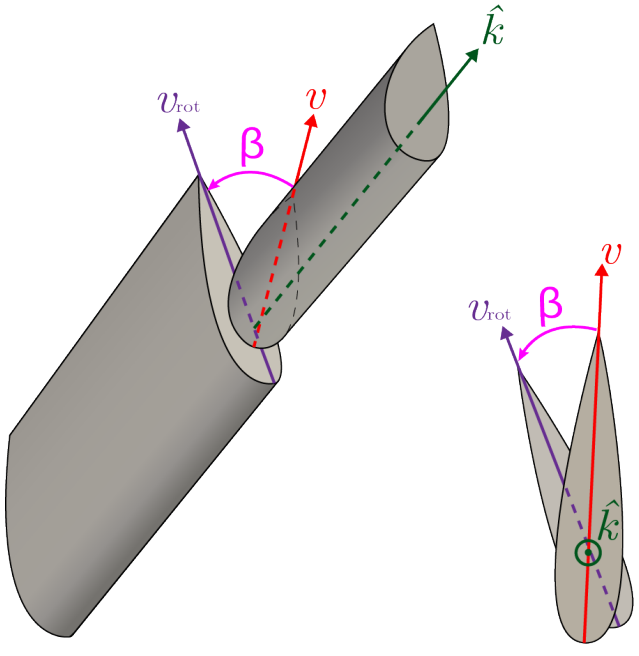


Figure 3. Illustration of blade pitching applied via Rodrigues' rotation formula. $\boldsymbol{v}$ represents the unpitched section of the blade, while $\boldsymbol{v}_{\text{rot}}$ represents the pitched section.

These steps are then repeated for each blade, as well as any struts (as applicable). Note that strut pitching is performed in a similar manner to blade pitching, albeit with a different initial tangent vector and unit axis of rotation.

https://doi.org/10.5194/wes-2026-205
Preprint. Discussion started: 4 November 2026
© Author(s) 2026. CC BY 4.0 License.



eawe european academy of wind energy
Open Access WIND ENERGY SCIENCE DISCUSSIONS

2.4 Data Analysis

2.4.1 Pitch Control Feasibility Criteria

An initial focus of pitch control in this study is to examine the ability of partial-span blade and/or strut pitch to control or regulate the rated power of the turbine in Region 3 operation. Typically, blade pitching is accomplished using the full length of the blade (as in HAWTs or H-type VAWTs). The pitchable troposkein-shaped design used in this study therefore poses a unique challenge, as only a partial blade span and/or full strut span are available for pitch control. Therefore, we examine feasibility of this application of pitch control, where feasibility of pitch control is characterized by three states:

- "Fully Feasible" if the rotor can maintain $C_{p,\max}$ until the rated power of 5 MW is obtained and subsequently can use pitch control to regulate that rated power.
- "Partially Feasible" if the rotor can maintain $C_{p,\max}$ for longer than it would relative to a stall-regulated rotor, but must initiate a reduction in TSR earlier than a Fully Feasible design in order to ensure it can control rated power at higher wind speeds.
- "Infeasible" if the rotor cannot use pitch control to maintain a consistent 5 MW rated power beyond the rated wind speed.

2.4.2 Annual Energy Production Calculation

AEP is chosen as a single metric that quantifies the impact of pitch control (versus the stall-regulated baseline) on power capture over the full range of operating wind speeds, calculated as follows (Fingersh et al., 2006):

$$\mathrm{AEP} = 8760 \times \sum_{u=5}^{25} W_u \cdot P_u \tag{9}$$

where W_u represents the probability of operating in wind speed u and P_u represents the power produced by the turbine at wind speed u. The Weibull distribution is defined as follows:

$$W(u) = \frac{k}{c}\left(\frac{u}{c}\right)^{(k-1)} \exp\left(-\left(\frac{u}{c}\right)^{k}\right) \tag{10}$$

$$c = \frac{\bar{u}}{\Gamma\left(1+\frac{1}{k}\right)} \tag{11}$$

where k is the Weibull shape factor (assumed to be 2.1), c is the Weibull scale factor (calculated as 10.16), $\bar{u}$ is the site-specific mean wind speed (chosen as $9\,\mathrm{m\,s^{-1}}$), and u is the wind inflow velocity.

2.4.3 Damage Equivalent Loads Calculation

Throughout its operational lifetime, the rotor experiences a wide range of wind speeds and loading conditions, each of which contributes to fatigue accumulation. Pitch control inevitably changes rotor loading patterns and thus affects the accumulated fatigue damage experienced by the turbine. Therefore, to properly quantify the structural impacts of pitch-controlled rotor

https://doi.org/10.5194/wes-2026-205
Preprint. Discussion started: 4 November 2026
© Author(s) 2026. CC BY 4.0 License.



eawe european academy of wind energy
Open Access WIND ENERGY SCIENCE DISCUSSIONS

strategies using one standardized metric, damage equivalent loads (DELs) are calculated for each design using the MLife fatigue post-processing tool (Hayman, 2012).

A DEL represents a hypothetical constant amplitude fatigue load that occurs at a fixed mean and frequency but produces the same equivalent lifetime fatigue damage as the full variable load spectrum experienced by the rotor (Thomsen, 1998; Freebury and Musial, 2000). The process of calculating the lifetime DEL is done in MLife using processed CACTUS loads time history data.

First, the aerodynamic forces — specifically the thrust (F_X), lateral load (F_Z), and torque (Q) — are extracted from a CACTUS simulation for a full rotation at each wind speed u. Only the last revolution of each CACTUS simulation is retained to ensure the simulation is fully converged.

Next, the time series of this revolution is extended by repeating the revolution 50 times, which ensures complete Rainflow cycle closure for the MLife processing step. MLife then takes this time series, performs Rainflow counting on the loading cycles, incorporates a Goodman correction using the tower base ultimate load capacity L_{ult}, and accumulates Weibull-weighted lifetime damage across all wind speeds, yielding a lifetime DEL at a reference frequency of $f_{\text{eq}} = 1.0$ Hz.

For the purposes of this comparative study, the DELs are computed assuming material properties of Glass Fiber Reinforced Polymer (GFRP) composite with a Wöhler exponent of 10. The Weibull parameters are chosen to match those of the AEP calculation in Sect. 2.4.2 and Eqs. (10)–(11). For the bending load channels (thrust F_X and lateral load F_Z), the tower base is an axisymmetric cylinder. Assuming an effective aerodynamic load center at mid-rotor height ($H/2$), the ultimate bending load capacity F_{ult} is identical in both transverse directions ($F_{X,\text{ult}} = F_{Z,\text{ult}} = F_{\text{ult}}$) and is determined from the beam bending equation:

$$\sigma = \frac{Mr}{I} = \frac{\left(F_{\text{ult}} \cdot \frac{H}{2}\right) r}{I} \implies F_{\text{ult}} = \frac{\sigma_{\text{ult}} I}{r\left(\frac{H}{2}\right)} \tag{12}$$

where I is the area moment of inertia, r is the outer radius of the tower base, and $\sigma_{\text{ult}} = 600$ MPa is a representative value chosen for the ultimate bending stress limit based on the values reported in Daniel and Ishai (2006).

For the torque load channel, the ultimate torque is derived from the shear stress equation for a hollow circular section:

$$\tau = \frac{Q\,r}{J} \implies Q_{\text{ult}} = \frac{S_{us} \cdot J}{r} \tag{13}$$

where J is the polar moment of inertia, r is the outer radius of the tower base, and $S_{us} = 70$ MPa is the assumed in-plane shear strength of the GFRP laminate based on standard composite material properties (Daniel and Ishai, 2006).

3 Results

Numerical simulations were conducted to evaluate the aerodynamic performance, structural loading, and fatigue behavior of the four rotor design cases—including the baseline stall-controlled case and the three pitch-controlled cases—for the UTD 5MW VAWT. To systematically identify the optimal actuation type and operating strategy, the analysis results are organized into three subsections:

https://doi.org/10.5194/wes-2026-205
Preprint. Discussion started: 4 November 2026
© Author(s) 2026. CC BY 4.0 License.



(1) Section 3.1 presents the operating strategy development, including RPM and pitch angle schedules versus wind speed and the resulting power curves for each operating strategy (partial-span blade-only pitch, strut-only pitch, and combined partial-span blade and strut pitching) to characterize the feasibility and operating behavior of each actuation case.

(2) Section 3.2 quantifies the AEP benefits of pitch control relative to the stall-regulated baseline.

(3) Section 3.3 examines the rotor loading impacts associated with these AEP gains, characterizing the peak and fatigue load changes introduced by implementing pitch control.

3.1 Operating Strategy Development and Feasibility of Pitch Control

Following the sequential methodology outlined in Sect. 2.3.1, operating strategies were developed for the baseline stall-regulated rotor and the three pitch-controlled configurations. The resulting rotor speed, tip speed ratio, power coefficient, and pitch angle schedules are shown in Fig. 4.

Figure 2(a) shows a typical Darrieus VAWT design, which has no pitch control capability. This rotor must rely entirely on aerodynamic stall behavior to regulate its rated power. From Fig. 4(a), it is evident that this behavior limits the range of operating speeds that the rotor experiences: the rotor speed increases only until $8\,\mathrm{m\,s^{-1}}$, capping off at a rated RPM value of approximately 7.0. From that point on, the rotor operates at the stall RPM.

Figures 2(b)–(d), by contrast, represent the newly developed pitchable VAWT designs explored in this work. These operating strategies no longer rely on stall to regulate the power, instead relying on pitch control. As seen in Fig. 4(a), this enables them to operate up to 8.6 RPM for the strut-only pitch case and up to 10.8 RPM for the blade-only and combined blade and strut pitch cases. This higher RPM corresponds to an extended operation under the optimal TSR (Fig. 4b), and, as a consequence, enables operation at $C_{p,\max}$ for a wider range of wind speeds (Fig. 4c).

Once the turbine reaches rated power, collective pitch control is engaged in Region 3 to maintain the 5 MW rating by pitching the blades and/or struts, as shown in Fig. 4(d). The blade-only and combined blade and strut cases pitch toward stall to shed lift and reduce aerodynamic torque, requiring maximum pitch angles of 52° and 36° at cut-out, respectively. By contrast, the strut-only pitching strategy relies on pitching the struts into deep drag regimes to produce counter-torque, requiring pitch angles up to 83° that ramp up rapidly above the rated wind speed. Unlike the blade-pitch cases, which use a combination of drag addition and lift reduction to lower the overall aerodynamic torque, the struts generate counter-torque entirely through the addition of drag. This means their pitch angles must advance rapidly above rated wind speed to produce sufficient counter-torque to maintain rated power, as C_D remains relatively flat until α exceeds approximately 20° (Appendix A and Fig. A1).

Pitch control feasibility evaluates the physical ability of pitchable blade and/or strut segments to regulate rated rotor power to the desired value (in this case, 5 MW). The feasibility of three different pitching strategies was evaluated relative to a stall-regulated baseline, including partial-span blade-only pitch, strut-only pitch, and combined partial-span blade and strut pitching. Feasibility of pitch control (Fully Feasible, Partially Feasible, and Infeasible) was determined according to the process in Sect. 2.4.1. The resulting power curves for each of the four operating strategies are shown in Fig. 5 for the 3-bladed rotor.

https://doi.org/10.5194/wes-2026-205
Preprint. Discussion started: 4 November 2026
© Author(s) 2026. CC BY 4.0 License.

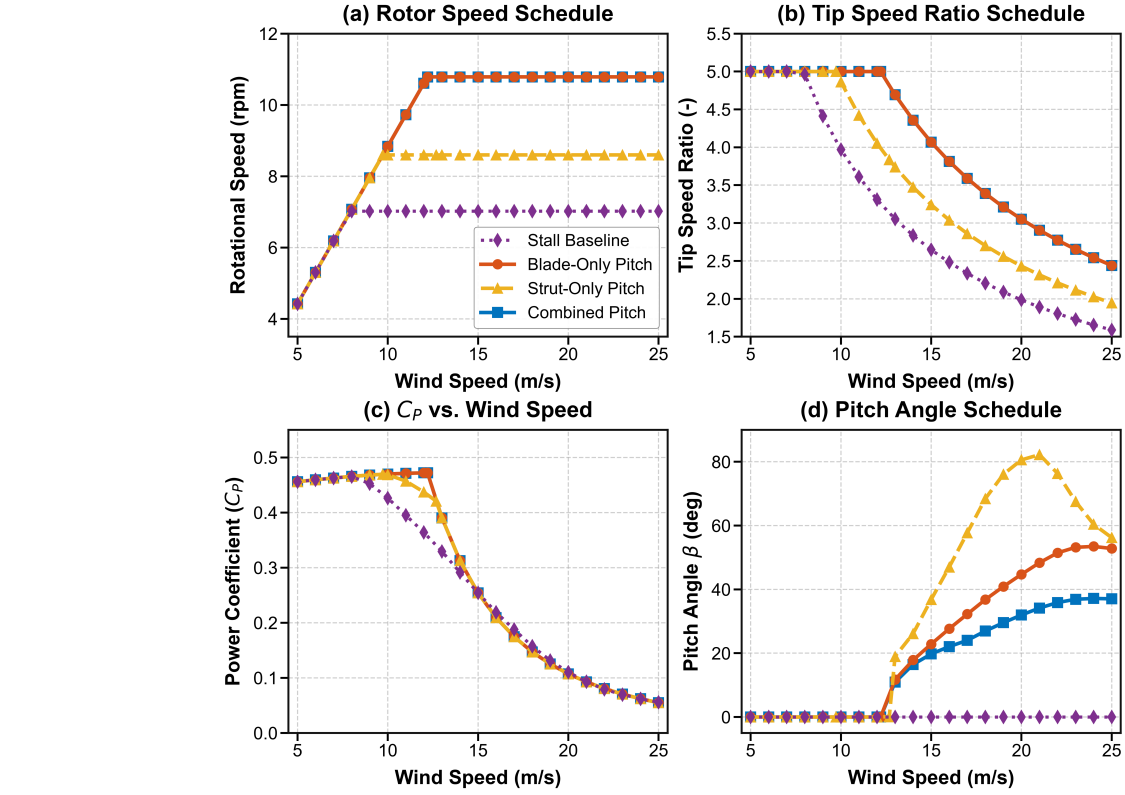


Figure 4. Operating strategies for the baseline stall-regulated and newly developed pitch-controlled rotor designs. Plotted parameters include (a) rotor speed schedule, (b) tip speed ratio schedule, (c) power coefficient (C_P), and (d) pitch angle vs. wind speed.

The combined blade and strut pitching method displays the highest viability for pitch-based power regulation. For this pitching mode, power regulation is Fully Feasible. That is, the strategy maintains $C_{p,\max}$ until the rated power of 5 MW is obtained, then further uses pitch control to sustain the rated power throughout all of Region 3 operation, as seen in Fig. 4(c)–(d). More specifically, this pitching strategy operates in Region 2 from cut-in ($5.0\,\mathrm{m\,s^{-1}}$) until rated ($12.2\,\mathrm{m\,s^{-1}}$), after which it operates entirely in Region 3 until cut-out (12.2–$25.0\,\mathrm{m\,s^{-1}}$). The blade-only pitching strategy is also Fully Feasible but requires larger pitch angles than the combined pitch case to maintain the power at 5 MW, as seen in Fig. 4(d).

On the other hand, the strut-only pitching strategy must reduce its operating RPM before hitting 5 MW rated power. If the rated RPM is set too high, the smaller pitchable strut lengths do not provide enough torque reduction to sufficiently control rotor power to 5 MW. Therefore, these models shift from constant TSR to constant RPM operation somewhere in-between the fully stall-regulated and fully pitch-controlled models (as seen in Fig. 4(a)–(b)). This means that the strut-only pitching strategy is Partially Feasible – operating entirely in Region 2 from $5.0\,\mathrm{m\,s^{-1}}$ until $9.7\,\mathrm{m\,s^{-1}}$, then in Region 2.5 from 9.7–$12.7\,\mathrm{m\,s^{-1}}$, and finally Region 3 from 12.7–$25.0\,\mathrm{m\,s^{-1}}$. The strut-only case must also increase its pitch angle more rapidly once rated power is reached (shown in Fig. 4d), as the magnitude of drag created by the struts does not become significant until an angle

https://doi.org/10.5194/wes-2026-205
Preprint. Discussion started: 4 November 2026
© Author(s) 2026. CC BY 4.0 License.



eawe european academy of wind energy
Open Access WIND ENERGY SCIENCE DISCUSSIONS

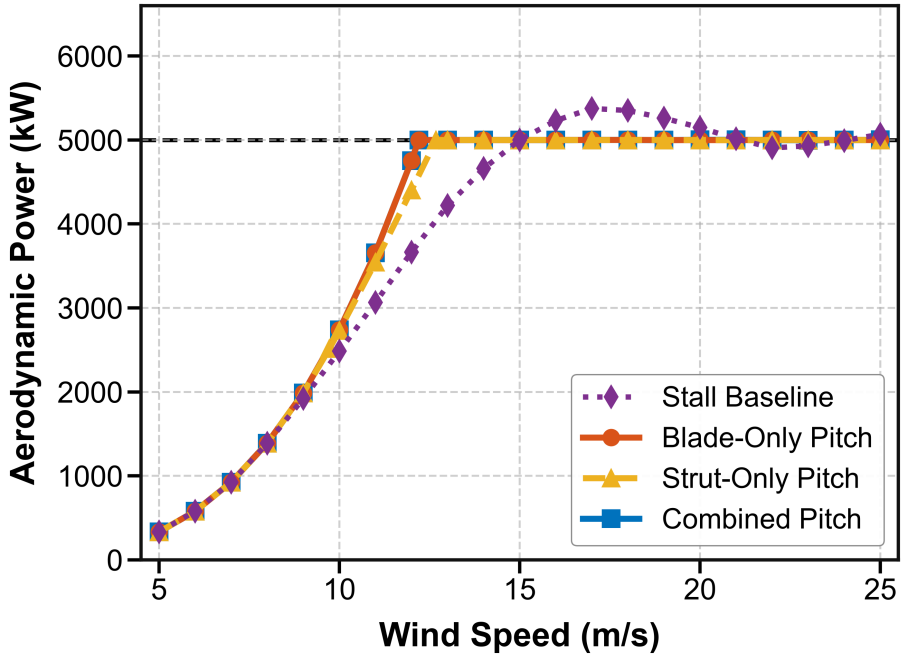


Figure 5. Power curves for the UTD 5MW 3-bladed VAWT across different pitching strategies.

of attack of around 20°. More information on the C_L and C_D polars for the airfoils used to model the blades and struts can be found in Appendix A.

3.2 Impact of Pitch Control on Annual Energy Production

AEP was determined according to the procedure noted in Sect. 2.4.2, and the resulting AEP gains of each operating strategy are shown in Fig. 6. Relative to the stall-regulated baseline, the pitch-controlled rotors see an AEP increase ranging from 6.62% (for strut-only pitching) to 8.05 % (for blade-only and combined blade and strut pitching). As seen in Sect. 3.1, the strut-only pitching case cannot maintain $C_{p,\max}$ as long as the blade-only or combined blade and strut cases, therefore leading to a smaller AEP increase. While the stall-regulated case reaches a maximum RPM of 7.0, the strut-only case increases its maximum RPM beyond that of the stall case to reach a rated speed of 8.6 RPM, and the blade-only and combined blade and strut cases both reach a maximum rated speed of 10.8 RPM.

In other words, pitch control increases the AEP of every turbine in the study, not through a direct power increase as a result of pitching, but rather through the aerodynamic control capability that pitching permits. Without collective pitch control, the rotor must begin stalling early on in its operating range — far before the rated power is attained. With active pitch control, however, the rotor can stay at an optimal TSR to maintain $C_{p,\max}$ for a much wider range of wind speeds and ultimately reach a higher rated RPM.

https://doi.org/10.5194/wes-2026-205
Preprint. Discussion started: 4 November 2026
© Author(s) 2026. CC BY 4.0 License.

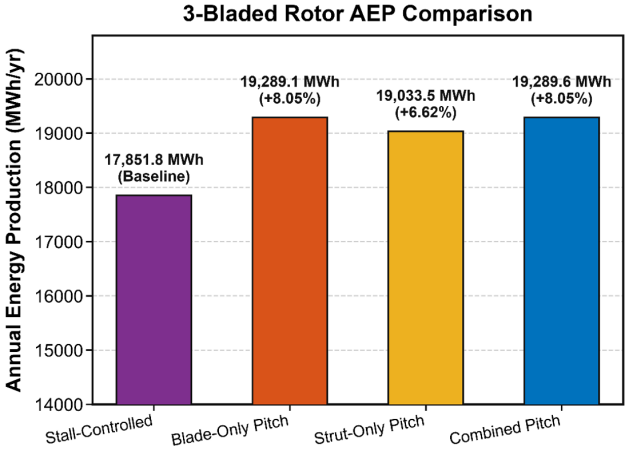


Figure 6. UTD 5MW 3-bladed VAWT AEP comparison for each pitching strategy.

To illustrate this point, the power coefficient as a function of wind speed, along with the site Weibull distribution, are plotted in Fig. 7. The blue shaded region represents the portion of the power curve where the pitch-controlled cases pick up additional energy. Extending Region 2 operation provides a significant boost to AEP because this region contains both a high probability of occurrence as well as a high power coefficient.

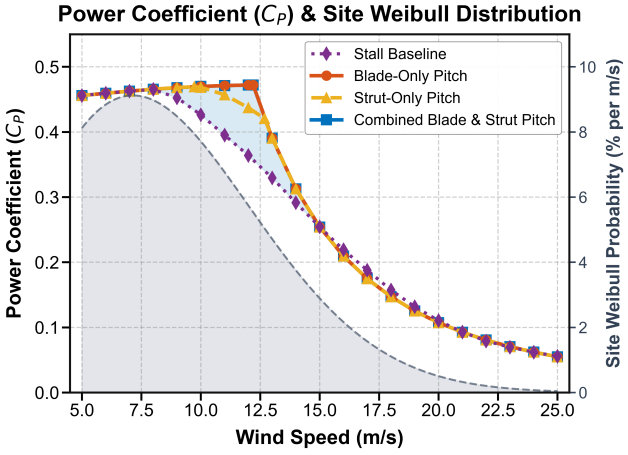


Figure 7. Power coefficient and site Weibull distribution for different pitching modes (3-bladed rotor).

3.3 Impacts of Pitch Control on Rotor Loads

In the prior section, pitch control applied to the troposkein-shaped Darrieus rotor was able to significantly increase power capture and AEP. Now, we turn our attention to analyzing the rotor loads — namely, the thrust, lateral, and torque loads. The

https://doi.org/10.5194/wes-2026-205
Preprint. Discussion started: 4 November 2026
© Author(s) 2026. CC BY 4.0 License.



eawe european academy of wind energy
Open Access WIND ENERGY SCIENCE DISCUSSIONS

primary quantities of interest are the peak loads and fatigue loads (as quantified via DELs) between the stall-regulated baseline and the various pitchable cases.

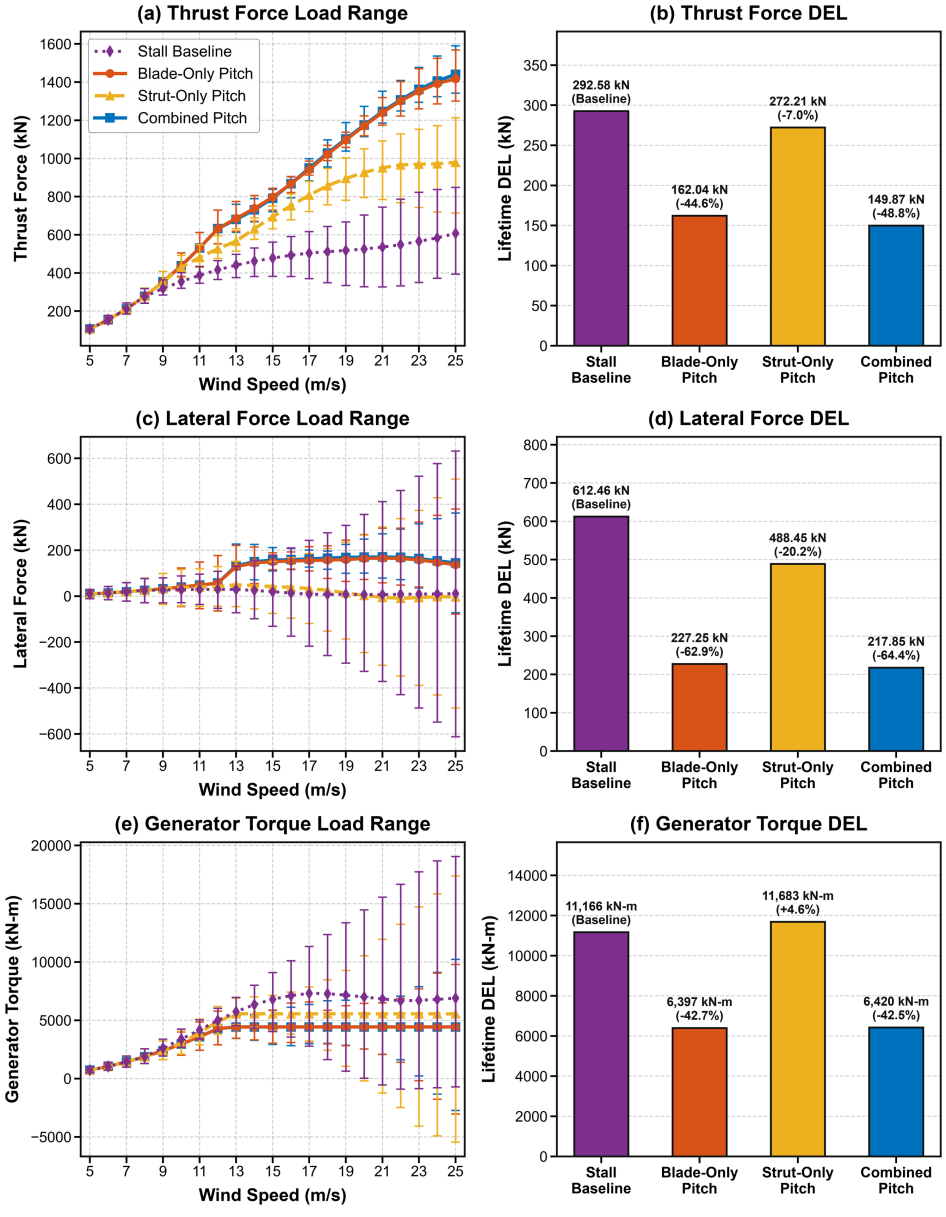


Figure 8. Load ranges and lifetime DELs for thrust, lateral, and torque loading on the UTD 5MW 3-bladed VAWT: (a) thrust force load range, (b) thrust force DEL, (c) lateral force load range, (d) lateral force DEL, (e) generator torque load range, and (f) generator torque DEL.

300 Figure 8(a) shows the impact of introducing pitch control on the thrust loads. When operating under the stall-controlled baseline, the mean thrust load reaches approximately 600 kN at 25 $\mathrm{m\,s^{-1}}$, peaking at a value above 800 kN. On the other hand,

https://doi.org/10.5194/wes-2026-205
Preprint. Discussion started: 4 November 2026
© Author(s) 2026. CC BY 4.0 License.



eawe european academy of wind energy
Open Access WIND ENERGY SCIENCE DISCUSSIONS

the strut-only pitching case reaches a mean thrust load of 1000 kN, peaking at 1200 kN, and the blade-only and combined blade and strut pitching reach a mean thrust load of 1400 kN with a peak just under 1600 kN. This demonstrates that all modes of pitch control lead to larger mean or peak thrust loads, which results from the higher RPM reached for those cases (see Fig. 4). However, one can note from Fig. 8(a) that despite the increases in mean and peak thrust loading, the loading fluctuations (magnitude of the minimum/maximum thrust loads within a revolution) for all three pitch control cases decrease. Damage equivalent loads (DELs) were computed to account for these changes in magnitude of both mean loads and alternating loads in order to quantify the fatigue loading changes of each pitch control case. The resulting thrust DEL changes are highlighted in Fig. 8(b).

Notably, the thrust DEL decreases nearly 50 % in the combined blade and strut pitching case when compared to the stall-regulated baseline. The blade-only pitching case shows significant reductions as well, dropping nearly 45 %. The reductions in DELs are driven primarily by reductions in the peak-to-peak alternating load magnitudes, despite the increase in mean loads. Further, the reduction of peak-to-peak alternating thrust loading arises mainly as a result of the higher RPM operation within the pitching cases. Though the higher RPM operation scales the peak thrust loading, it also decreases the variation in angle of attack experienced by the equatorial (non-pitching) sections of the rotor, which in turn decreases thrust load variation. Given that the strut-only pitching case does not increase its RPM as much as the blade-only case does, the azimuthal variation remains larger in comparison, and thus the reduction in the thrust DEL is smaller.

In addition to reduced azimuthal variation due to higher RPM operation, blade pitching itself also serves to reduce the thrust DEL. Blade pitching simultaneously decreases the peak loading experienced during the upwind pass and increases the minimum loading experienced during the crosswind pass, flattening the rotor thrust profile across the azimuthal range. Strut pitching, by contrast, does not shed sectional lift; instead, the struts act as flat bluff bodies by which drag is imparted on the rotor without affecting the lift of any main blade sections.

Figure 8(c) breaks down the lateral loads as a function of wind speed for each operating strategy. Interestingly, the strut-only pitching case tracks a mean load very close to the stall-regulated baseline (near-zero). However, the loading fluctuations of this case are reduced slightly relative to the baseline. On the other hand, the blade-only and combined blade and strut pitch cases deviate to a non-zero lateral load mean. This behavior is consistent with the lateral wake deflection due to pitching observed in Ribeiro et al. (2024). This can be explained by analyzing the projection of normal and tangential forces across the crosswind Z-axis:

$$F_Z(\theta) = F_T(\theta)\sin(\theta) + F_N(\theta)\cos(\theta) \tag{14}$$

where F_N and F_T are defined in Eqs. (4)–(5). In the stall-regulated baseline, $F_T(\theta)$ and $F_N(\theta)$ maintain relative symmetry about the streamwise X-axis, and thus their contributions to F_Z tend to cancel over a full revolution. On the other hand, the pitch-controlled strategies alter this symmetry through two main mechanisms. First, maintaining a higher rated rotor speed enables the rotor to operate at higher tip speed ratios relative to the stall-regulated baseline, narrowing the range of angles of attack that each blade experiences. Second, active blade pitching modifies the local angle of attack on actuated sections as $\alpha = \psi + \beta$ (Eq. 1). Because the inflow angle ψ varies strongly with azimuth—positive in the upwind pass, and negative in the

https://doi.org/10.5194/wes-2026-205
Preprint. Discussion started: 4 November 2026
© Author(s) 2026. CC BY 4.0 License.



eawe european academy of wind energy
Open Access WIND ENERGY SCIENCE DISCUSSIONS

downwind pass—prescribing a fixed pitch angle β causes the angle of attack α to shift into different lift and drag regimes of the airfoil polars throughout the rotation, and likewise causes the rotor to experience a non-zero mean angle of attack across a full revolution. The variation in angle of attack shifts $C_L(\alpha)$ and $C_D(\alpha)$ (Eqs. 2–3), and consequently F_N and F_T (Eqs. 4–5), asymmetrically around the azimuth, breaking the symmetry that kept the lateral force F_Z at a near-zero mean.

The primary source of negative F_Z in the downwind pass comes from the $F_T \sin(\theta)$ term, which is negative throughout $180° < \theta < 360°$. In the baseline, this is further compounded in the quadrant from $270° < \theta < 360°$ by the $F_N \cos(\theta)$ term. Although $\cos(\theta) > 0$ here, $F_N < 0$ due to the strongly negative angles of attack experienced in this region, making the product $F_N \cos(\theta) < 0$ as well. The higher operating tip speed ratio serves to reduce the cyclic variation in the inflow angle ψ, while active blade pitch modifies the angle of attack α throughout the downwind pass, which reduces the negative contributions from these terms and allows the positive lateral forces generated during the upwind pass to dominate the cycle. This keeps the lateral load across the azimuth in a positive mean value, and simultaneously reduces the fluctuations in lateral loading, which provides further benefits for fatigue.

Much like those of the thrust loading, the cyclic fluctuations of the lateral load are reduced significantly for all three pitch control cases. This effect is more pronounced for the blade-only and combined blade and strut pitching cases, but the strut-only pitching case shows some reduction as well. The reduced oscillatory loading furthermore drops the lateral load DELs by approximately 63–64 % in the blade-only and combined blade and strut pitching cases, while the strut-only case achieves a more modest reduction around 20 %, consistent with its lower operating RPM. These lateral load ranges and DELs are illustrated in Fig. 8(d).

Figure 8(e) shows the generator torque of the rotor for each operating strategy. Note that as the average RPM in Region 3 increases, the mean torque drops to match the rotor power ($P = Q\omega$) to 5 MW. Once again, the magnitude of the peak loading drops for the torque loading. For the blade-only and combined blade and strut pitching cases, the oscillatory torque loading is also significantly reduced. By pitching the blade segments toward stall, the cyclic variation in tangential force is smoothed across the azimuth (Eq. 5), yielding generator torque DEL reductions of nearly 43 % versus the stall-regulated baseline. The strut-only pitching case, by contrast, relies on drag-based counter-torque from the struts rather than direct reduction of blade tangential force fluctuations. This method of torque reduction does not suppress cyclic torque variation as effectively, and the more modest RPM increase of the strut-only case provides less cyclic smoothing than the blade-pitched designs. As a result, the strut-only generator torque DEL increases slightly by 4.6 % relative to the stall-regulated baseline. The generator torque DELs for all four operating strategies are shown in Fig. 8(f).

3.4 Results Summary

Table 2 consolidates the key performance metrics — namely, AEP, peak loads, and DELs — for the 3-bladed rotor across all operating strategies. Pitch control delivers a consistent dual benefit relative to the stall-regulated baseline: AEP increases by 6–8 % across each strategy, and peak lateral and torque loads decrease for all pitched designs. Fatigue loads (DELs) are reduced substantially for the thrust and lateral load channels across all pitching strategies, as well as the generator torque load in the blade-only and combined blade and strut pitching cases. The primary structural penalty exhibited by the pitched cases

https://doi.org/10.5194/wes-2026-205
Preprint. Discussion started: 4 November 2026
© Author(s) 2026. CC BY 4.0 License.



eawe european academy of wind energy
Open Access WIND ENERGY SCIENCE DISCUSSIONS

370 is an increase in peak thrust, which occurs as a direct consequence of higher RPM operation in Region 3 (discussed further in Sect. 4).

Table 2. Peak loads ($25\,\mathrm{m\,s^{-1}}$), 20-year lifetime DELs, and AEP for the 3-bladed rotor. Percent changes are relative to the stall-regulated baseline.

Pitching Mode	AEP (MWh/yr)	Thrust Load, F_X (kN)		Lateral Load, F_Z (kN)		Generator Torque, Q (kN·m)	
		Peak	DEL	Peak	DEL	Peak	DEL
Stall Baseline	17 852 (+0.00 %)	847.9 (+0.00 %)	292.6 (+0.00 %)	631.6 (+0.00 %)	612.5 (+0.00 %)	19 050 (+0.00 %)	11 166 (+0.00 %)
Blade-Only Pitch	19 289 (+8.05 %)	1568 (+84.9 %)	162.0 (−44.6 %)	379.2 (−39.9 %)	227.3 (−62.9 %)	9783 (−48.6 %)	6397 (−42.7 %)
Strut-Only Pitch	19 034 (+6.62 %)	1213 (+43.1 %)	272.2 (−7.0 %)	509.4 (−19.3 %)	488.5 (−20.2 %)	17 390 (−8.7 %)	11 683 (+4.6 %)
Combined Pitch	19 290 (+8.05 %)	1591 (+87.6 %)	149.9 (−48.8 %)	361.7 (−42.7 %)	217.9 (−64.4 %)	10 230 (−46.3 %)	6420 (−42.5 %)

Among the three pitching strategies, blade-only and combined blade and strut pitching deliver the most significant improvements across all metrics. The strut-only case provides more modest improvements and uniquely shows a minor increase in the generator torque DEL, as discussed in Sect. 3.3. Still, the strut-only pitching case shows interesting behavior that may in fact 375 be more favorable in some cases, achieving a significant AEP increase while maintaining the peak thrust load increase at a level only half that of the blade-pitched cases.

Finally, a comparison with an aerodynamically equivalent UTD 5MW 2-bladed VAWT rotor reveals that while the AEP gains due to pitch control are nearly identical to those of the 3-bladed rotor, fatigue load behavior fundamentally differs. Whereas the 3-bladed rotor exhibits significant DEL reductions, the 2-bladed rotor shows DEL increases under pitch control. 380 More information on this behavior is presented in Appendix B.

4 Discussion

Partial-span blade and strut pitch control shows incredible ability to regulate the power of the troposkein-shaped Darrieus VAWT. Not only does the rotor obtain the ability to regulate power to 5 MW beyond the rated wind speed, but it also greatly increases power production in below-rated conditions, as the rotor is able to maintain $C_{p,\max}$ for a much larger range of wind 385 speeds relative to the stall-regulated baseline. This results in a significant AEP increase for all pitch-controlled cases. These benefits mainly arise from the increased RPM operation associated with pitching strategies. In other words, pitch control in and of itself does not produce a direct increase in power production, but rather introduces significant aerodynamic control capability which enables the rotor to operate at higher RPMs to capture more power while still regulating power at higher wind speeds. However, as seen in the previous section, this increased RPM operation has significant impacts on loading. Higher- 390 RPM operation simultaneously increases peak thrust loading while reducing peak lateral and torque loading; meanwhile, all oscillatory load magnitudes (and their associated DELs) decrease among the three primary load channels investigated.

Higher-RPM operation has two cascading impacts which physically drive loading changes in the rotor. First, higher-RPM operation increases the magnitude of relative velocity V_{rel} for any given airfoil section, following from the increased contribu-

https://doi.org/10.5194/wes-2026-205
Preprint. Discussion started: 4 November 2026
© Author(s) 2026. CC BY 4.0 License.



eawe european academy of wind energy
Open Access WIND ENERGY SCIENCE DISCUSSIONS

tion of the turbine rotational velocity. This increase in V_{rel} directly scales the aerodynamic forces (Eqs. 2–5), and is the primary driver of increased peak loads in Region 3. Second, the increased rotational velocity seen by the airfoil section leads to smaller angle of attack variation, as the larger rotational component comprising V_{rel} necessarily reduces the relative influence of the freestream wind on the angle ψ (Eq. 1).

Importantly, however, the effect of the pitch angle β on angle of attack is spatially non-uniform across the rotor. At the equatorial blade sections, no blade pitch is applied, meaning that high RPM operation serves purely to reduce the variation in angle of attack (and in turn, the oscillatory loading and DELs). By contrast, the pitchable blade and strut segments experience a larger mean angle of attack in Region 3, which intentionally induces stall or increases drag to counteract the excess torque produced by the equatorial sections. The effect of higher-RPM operation, coupled with the spatially dependent effect of blade pitch, simultaneously drives the reduced oscillatory loading and increased peak loading observed across all pitching strategies in Fig. 8.

Figure 9 illustrates the impacts of each pitch control strategy on the angle of attack of an equatorial blade section. Wind speeds ranging from 10 to 25 $\mathrm{m\,s^{-1}}$ are selected to showcase the variation at different wind speed, RPM, and pitch angle combinations. Note that wind speeds below 9 $\mathrm{m\,s^{-1}}$ will show identical angle of attack variation between pitching cases due to overlap in the operating strategy at low wind speeds, and that the blade-only and combined blade and strut pitching cases show identical angle of attack at *all* wind speeds as they operate at the same RPM.

At the lower wind speeds, the equatorial angle of attack of each operating strategy does not differ significantly. Even the stall-regulated baseline has little variation, staying well within the linear (pre-stall) region of the airfoil polar. However, at a wind speed of 15 $\mathrm{m\,s^{-1}}$, the stall-regulated baseline approaches angles of attack where the airfoil begins to stall. Due to the increased RPM operation of the pitch-controlled strategies, the angle of attack variation is reduced. The degree of this reduction varies between pitching strategies in proportion to their respective operating RPMs: the strut-only pitching case reaches a lower maximum RPM than the blade-only and combined blade and strut pitching cases (Fig. 4), resulting in a correspondingly larger angle of attack variation at the equator. Meanwhile, the blade-only and combined blade and strut pitching cases operate at identical RPMs to each other and thus show identical equatorial angle of attack profiles. At the equatorial blade segment, the angle of attack variation for the pitched cases is kept at angles near or below stall, whereas the stall-regulated baseline greatly exceeds the stall point. This is also the primary driver of the increased peak thrust load but reduced fatigue loads: tracing the evolution of thrust in Eqs. (2)–(7), one can see the dependence on both the relative velocity V_{rel} and angle of attack α. As V_{rel} increases due to the higher RPM, so does the peak thrust force, but as the variation in α decreases, so too does the oscillation in thrust force.

The primary mechanism by which the rotor regulates power in Region 3 differs between operating strategies. The stall-regulated baseline operates at a lower RPM and does not vary the pitch angle β. As such, the stall-regulated baseline operates within the linear region of the C_L vs. α curve at lower wind speeds and enters deep stall at higher wind speeds.

On the other hand, the blade-only pitching strategy operates with its equatorial sections mainly in the pre-stall region, even at higher wind speeds. Thus, this pitching strategy requires large pitch angles at higher wind speeds to bring the pitchable blade segments to deep stall in almost the entire azimuth range, counteracting the increased torque contribution from the fast-

https://doi.org/10.5194/wes-2026-205
Preprint. Discussion started: 4 November 2026
© Author(s) 2026. CC BY 4.0 License.

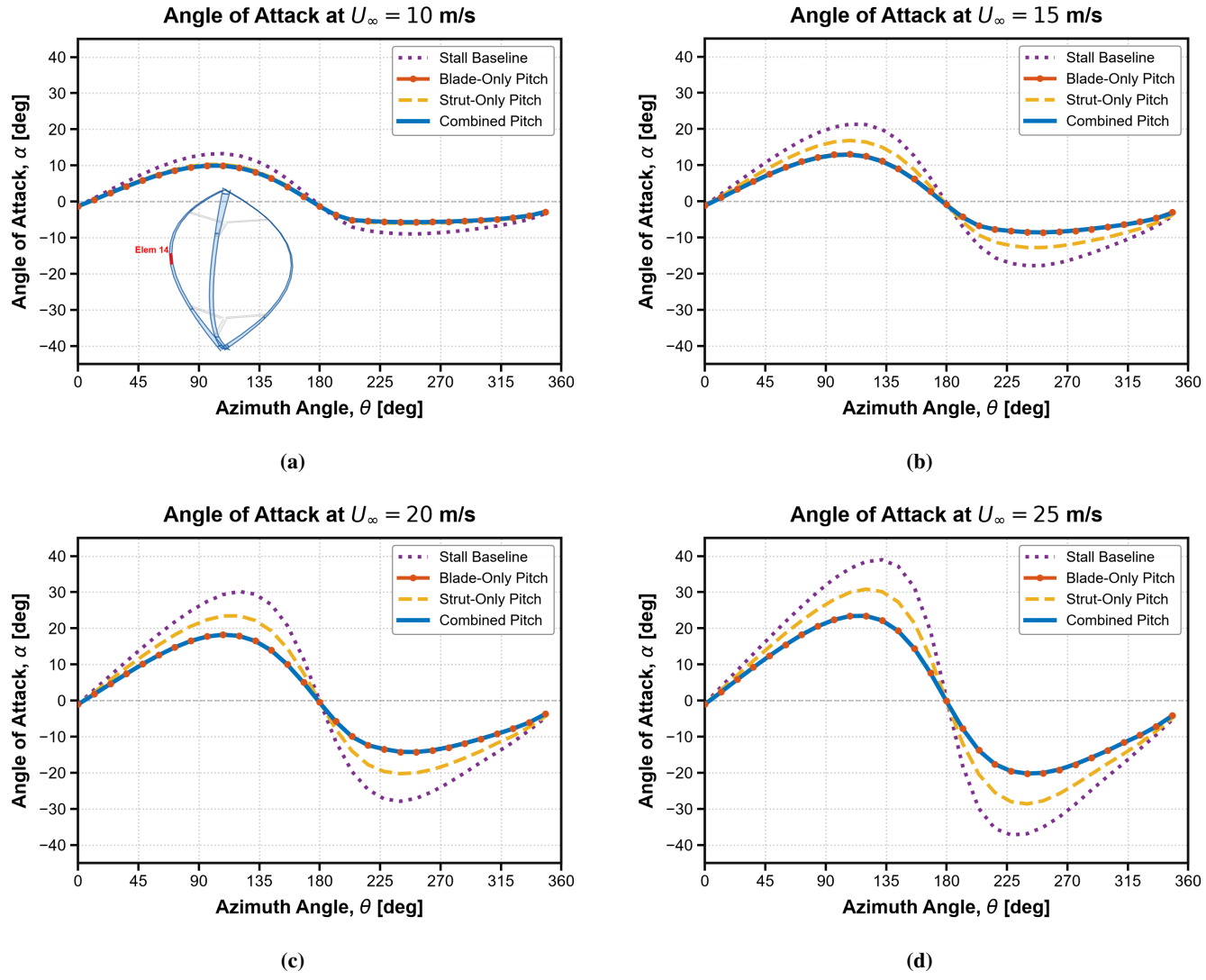


Figure 9. Angle of attack vs. azimuth at the equator for all four operating strategies. Plots are shown for wind speeds of (a) $10\,\mathrm{m\,s^{-1}}$, (b) $15\,\mathrm{m\,s^{-1}}$, (c) $20\,\mathrm{m\,s^{-1}}$, and (d) $25\,\mathrm{m\,s^{-1}}$.

https://doi.org/10.5194/wes-2026-205
Preprint. Discussion started: 4 November 2026
© Author(s) 2026. CC BY 4.0 License.



spinning equatorial sections. The strut-only pitching strategy enters stall at some angles of attack in the higher wind speeds, but requires constant pitching of the struts to induce a drag-based counter-torque against the positive torque from its equatorial blade sections. The combined blade and strut case uses a combination of both methods, simultaneously reducing the torque contribution from pitchable blade segments and introducing pure drag counter-torque from the pitchable strut segments.

5 Conclusions

In this study, pitch control is applied to the operation of troposkein-shaped Darrieus VAWTs under collective partial blade span and/or strut pitch control – a mode of operation previously restricted to HAWTs and H-type VAWTs. Power regulation of the troposkein VAWT is found to be feasible using only a small pitchable portion of the rotor blades and/or struts. Furthermore, the effects of pitch control on AEP, peak loads, and fatigue loads have been analyzed. The key findings are summarized as follows:

- Power regulation of a troposkein-shaped Darrieus VAWT is feasible by converting less than half of the total blade length to pitchable segments. Many strategies — including blade-only pitch control, strut-only pitch control, and combined blade and strut pitch control — can be used to regulate the power to 5 MW.
- Troposkein pitch control can increase the annual energy production of a rotor by 6–8 % for a site with a mean wind speed of $9\,\mathrm{m\,s^{-1}}$, depending on the pitching implementation used.
- The increased RPM operation resulting from converting to a pitch-controlled strategy increases peak thrust loads on the rotor but decreases peak lateral and torque loads.
- The oscillatory loads for thrust, lateral, and torque loadings are also reduced, resulting in significant reductions in lifetime DELs in all the principal design loads.

The application of pitch control to a troposkein-shaped Darrieus VAWT has never been studied prior to this work. Operating as a pitch-controlled VAWT allows the troposkein to maintain its structural benefits over the H-type VAWT at larger scales while boosting power and significantly reducing rotor fatigue loads. At the same time, these benefits come from converting a stall-regulated design into a pitch-controlled one rather than optimizing a design for pitch control from the ground up, implying that even more benefit can be obtained from the pitch-controlled troposkein VAWT with the combination of aerodynamic design and design of pitch control. Future work should thus seek to optimize the airfoils, chord, and baseline operating strategies directly for pitch control, in addition to investigating how the peak loading associated with troposkein pitch control can be reduced.

Code availability. The CACTUS simulation code is an open-source tool developed by Sandia National Laboratories and is available at https://github.com/sandialabs/CACTUS. Post-processing and fatigue analysis scripts utilize the NREL MLife tool available at https://www.nlr.gov/wind/nwtc/mlife.

https://doi.org/10.5194/wes-2026-205
Preprint. Discussion started: 4 November 2026
© Author(s) 2026. CC BY 4.0 License.



eawe european academy of wind energy
Open Access WIND ENERGY SCIENCE DISCUSSIONS

Data availability. The simulation data supporting the findings of this study are available from the corresponding author upon reasonable request.

Appendix A: Airfoil Polars for Blades and Struts

The aerodynamic performance of the NACA 0021 airfoil, used for both the blade and strut elements of the UTD 5MW model, is characterized by the lift and drag polars shown in Fig. A1. These polars are used directly in the CACTUS simulations to compute sectional lift and drag forces as a function of angle of attack α (Eqs. 2–3).

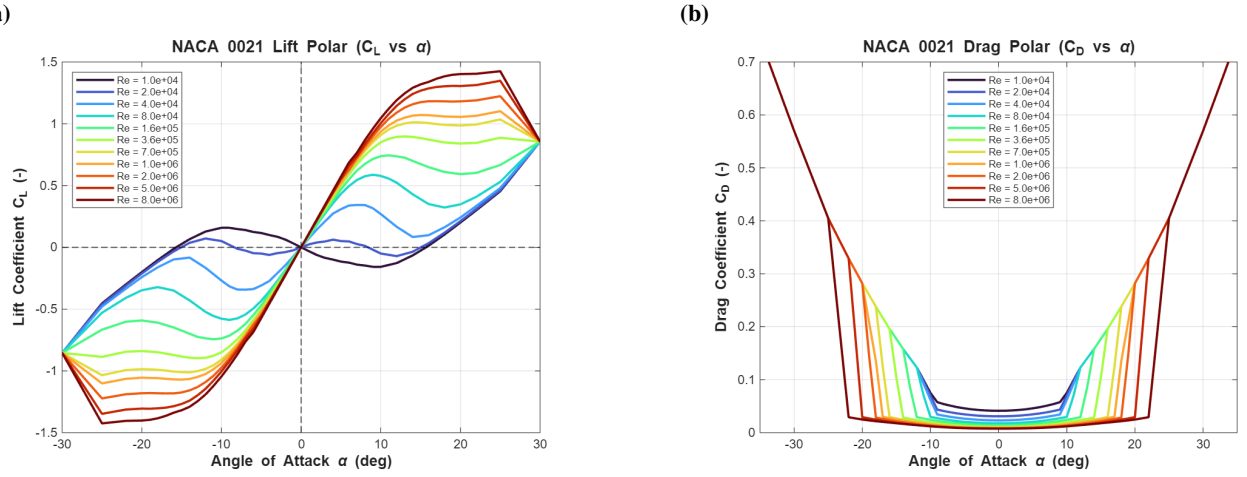


Figure A1. NACA 0021 airfoil polars used for blade and strut elements in CACTUS: (a) lift coefficient C_L vs. angle of attack α; (b) drag coefficient C_D vs. angle of attack α.

Appendix B: 2-Bladed Rotor Results

This section presents the results for the 2-bladed UTD 5MW rotor across all four operating strategies. The 2-bladed rotor maintains an identical swept area, rotor radius, tower height, and rated power as the 3-bladed case, while increasing chord lengths across the blades by 1.5× to preserve identical rotor solidity. The results for pitch feasibility, effects on AEP, and effects on loads are summarized below. (For the interested reader, more details on the design and analysis of the UTD 5MW 2- and 3-bladed VAWT rotors can be found in Sakib and Griffith (2022)).

Feasibility: The feasibility of pitch control for the 2-bladed rotor mirrors that of the 3-bladed rotor. The blade-only and combined blade and strut pitching cases are Fully Feasible, maintaining a constant 5.0 MW rated power from the rated wind speed up to cut-out, with maximum pitch angles of $51.65°$ and $36.02°$, respectively. The strut-only case remains Partially Feasible, with a maximum pitch angle of $83°$. The stall-regulated 2-bladed rotor reaches a maximum RPM of 6.95, the strut-only case reaches 8.73 RPM, and the blade-only and combined blade and strut pitching cases both reach 11.32 RPM.

https://doi.org/10.5194/wes-2026-205
Preprint. Discussion started: 4 November 2026
© Author(s) 2026. CC BY 4.0 License.



eawe european academy of wind energy
Open Access WIND ENERGY SCIENCE DISCUSSIONS

Annual Energy Production: The AEP gains of the 2-bladed pitch-controlled rotors are nearly identical to those of the 3-bladed rotors. The stall-regulated 2-bladed rotor produces $17\,867\,\mathrm{MWh\,yr^{-1}}$, whereas the strut-only pitching case produces $19\,064\,\mathrm{MWh\,yr^{-1}}$ (+6.70 %) and the blade-only and combined pitching cases both produce $19\,323\,\mathrm{MWh\,yr^{-1}}$ (+8.15 %). This agreement in AEP gains across blade counts indicates that the energy capture benefit of pitch control is independent of the number of blades.

Peak and Fatigue Loads: Unlike the 3-bladed case, where pitch control produced significant reductions in fatigue loads, the 2-bladed rotor exhibits increases in both peak loads and DELs across all pitching strategies and all load channels. These results are summarized in Table B1.

Table B1. Peak loads ($25\,\mathrm{m\,s^{-1}}$), 20-year lifetime DELs, and AEP for the 2-bladed rotor. Percent changes are relative to the stall-regulated baseline.

Pitching Mode	AEP (MWh/yr)	Thrust Load, F_X (kN)		Lateral Load, F_Z (kN)		Generator Torque, Q (kN·m)	
		Peak	DEL	Peak	DEL	Peak	DEL
Stall Baseline	17 867 (+0.00 %)	1085 (+0.00 %)	712.6 (+0.00 %)	1245 (+0.00 %)	1208 (+0.00 %)	14 860 (+0.00 %)	11 038 (+0.00 %)
Blade-Only Pitch	19 323 (+8.15 %)	2169 (+100.0 %)	1228 (+72.3 %)	1380 (+10.8 %)	1383 (+14.5 %)	24 450 (+64.5 %)	22 056 (+99.8 %)
Strut-Only Pitch	19 064 (+6.70 %)	1596 (+47.1 %)	894.3 (+25.5 %)	1280 (+2.8 %)	1282 (+6.1 %)	15 950 (+7.3 %)	17 540 (+58.9 %)
Combined Pitch	19 323 (+8.15 %)	2290 (+111.1 %)	1284 (+80.2 %)	1413 (+13.5 %)	1324 (+9.6 %)	25 010 (+68.3 %)	22 412 (+103.0 %)

As seen in the table, the thrust, lateral, and generator torque DELs all increase substantially, with the generator torque DEL nearly doubling for the blade-only and combined pitching cases. This result contrasts sharply with the 3-bladed results, where the blade-only and combined cases yielded DEL reductions of approximately 43–65 % depending on the load channel. The difference arises from the cyclic load fluctuations in the 2-bladed rotor. While the 3-bladed configuration benefits from a load-averaging effect across blades that reduces oscillatory loading, the 2-bladed rotor's cyclic loads are amplified by the higher RPM operation in the same way as described in Section 4. Because of the 2-bladed rotor's 180° blade spacing, the blades alternately cycle through their peak and near-zero loading zones every 180° of rotation, producing a strong 2P oscillation with no cancellation between blades. As a result, the increased mean loads from pitch control compound with the already-large alternating loads, driving up the lifetime DELs rather than reducing them.

Author contributions. This work was performed during the PhD research of DB under the supervision of DTG as part of an Advanced Research Projects Agency–Energy (ARPA-E)-funded project named "A Low-Cost Offshore Floating Power Generation System for Energy-Efficient Underwater Data". DB and DTG contributed to the analysis and interpretation of the data, and the paper was prepared by DB with the help of DTG.

Competing interests. The authors declare that they have no conflict of interest.

https://doi.org/10.5194/wes-2026-205
Preprint. Discussion started: 4 November 2026
© Author(s) 2026. CC BY 4.0 License.



Acknowledgements. The research presented herein was funded by the US Department of Energy Advanced Research Projects Agency-Energy (ARPA-E) under the ATLANTIS program with project title "A Low-Cost Offshore Floating Power Generation System for Energy-Efficient Underwater Data" with Award No. DE-AR0001179. Any opinions, findings, and conclusions or recommendations expressed in this material are those of the authors and do not necessarily reflect the views of ARPA-E. The authors are grateful for the support of the ARPA-E program and staff, and the project team. The first author also recognizes the UT Dallas Eugene McDermott Graduate Fellowship program (award number 202303) for providing financial support for his research.

https://doi.org/10.5194/wes-2026-205
Preprint. Discussion started: 4 November 2026
© Author(s) 2026. CC BY 4.0 License.



eawe european academy of wind energy
Open Access WIND ENERGY SCIENCE DISCUSSIONS

References

Bensason, D., Mulay, J., Sciacchitano, A., and Ferreira, C.: Experimental demonstration of regenerative wind farming using a high-density layout of vertical-axis wind turbines, Wind Energy Science, 10, 1499–1528, https://doi.org/10.5194/wes-10-1499-2025, 2025.

Bianchini, A., Balduzzi, F., Di Rosa, D., and Ferrara, G.: On the use of Gurney Flaps for the aerodynamic performance augmentation of Darrieus wind turbines, Energy Conversion and Management, 184, 402–415, https://doi.org/10.1016/j.enconman.2019.01.068, 2019.

Bourhis, M., Pereira, M., and Ravelet, F.: Experimental investigation of the effects of the Reynolds number on the performance and near wake of a wind turbine, Renewable Energy, 209, 63–70, https://doi.org/10.1016/j.renene.2023.03.093, 2023.

Brownstein, I. D., Kinzel, M., and Dabiri, J. O.: Performance enhancement of downstream vertical-axis wind turbines, Journal of Renewable and Sustainable Energy, 8, https://doi.org/10.1063/1.4964311, 2016.

Daniel, I. M. and Ishai, O.: Engineering Mechanics of Composite Materials, Oxford University Press, New York, 2nd edn., 2006.

Daraee, M. A. and Abbasi, S.: A novel approach to performance improvement of a VAWT using plasma actuators, Journal of Cleaner Production, 424, 138 876, https://doi.org/10.1016/j.jclepro.2023.138876, 2023.

De Tavernier, D., Ferreira, C., and Goude, A.: Vertical-Axis Wind Turbine Aerodynamics, p. 1317–1361, Springer International Publishing, ISBN 9783030313074, https://doi.org/10.1007/978-3-030-31307-4_64, 2022.

Fingersh, L., Hand, M., and Laxson, A.: Wind Turbine Design Cost and Scaling Model, https://doi.org/10.2172/897434, 2006.

Freebury, G. and Musial, W.: Determining Equivalent Damage Loading for Full-Scale Wind Turbine Blade Fatigue Tests, in: 19th ASME Wind Energy Symposium, p. 50, Reno, NV, https://doi.org/10.2514/6.2000-50, 2000.

Greenblatt, D., Schulman, M., and Ben-Harav, A.: Vertical axis wind turbine performance enhancement using plasma actuators, Renewable Energy, 37, 345–354, https://doi.org/10.1016/j.renene.2011.06.040, 2012.

Gupta, A., Abderrahmane, H. A., and Janajreh, I.: Flow analysis and sensitivity study of vertical-axis wind turbine under variable pitching, Applied Energy, 358, 122 648, https://doi.org/10.1016/j.apenergy.2024.122648, 2024.

Hayman, G.: MLife Theory Manual for Version 1.00, Tech. Rep. 75, 2012.

Jafari, M., Sakib, M. S., Griffith, D. T., Brownstein, I., Strom, B., and Cooney, J.: Wind Tunnel Experiment to Study Aerodynamics and Control of H-Rotor Vertical Axis Wind Turbine, Journal of Physics: Conference Series, 2265, 022 084, https://doi.org/10.1088/1742-6596/2265/2/022084, 2022.

Kirke, B. K. and Lazauskas, L.: Enhancing the Performance of Vertical Axis Wind Turbine Using a Simple Variable Pitch System, Wind Engineering, 15, 187–195, https://www.jstor.org/stable/43750355, 1991.

Le Fouest, S. and Mulleners, K.: Optimal blade pitch control for enhanced vertical-axis wind turbine performance, Nature Communications, 15, https://doi.org/10.1038/s41467-024-46988-0, 2024.

McConnell, R. D.: Giromill Overview, https://doi.org/10.2172/6046045, 1979.

Miller, M. A., Duvvuri, S., Brownstein, I., Lee, M., Dabiri, J. O., and Hultmark, M.: Vertical-axis wind turbine experiments at full dynamic similarity, Journal of Fluid Mechanics, 844, 707–720, https://doi.org/10.1017/jfm.2018.197, 2018.

Murray, J. and Barone, M.: The Development of CACTUS, a Wind and Marine Turbine Performance Simulation Code, in: 49th AIAA Aerospace Sciences Meeting including the New Horizons Forum and Aerospace Exposition, American Institute of Aeronautics and Astronautics, https://doi.org/10.2514/6.2011-147, 2011.

Murray, R. M., Li, Z., and Sastry, S. S.: A Mathematical Introduction to Robotic Manipulation, chap. 2, pp. 27–28, CRC Press, Boca Raton, FL, 1994.

https://doi.org/10.5194/wes-2026-205
Preprint. Discussion started: 4 November 2026
© Author(s) 2026. CC BY 4.0 License.



Paraschivoiu, I., Ammar, S., and Saeed, F.: VAWT versus HAWT: a comparative performance study of 2–6 MW rated capacity turbines, Transactions of the Canadian Society for Mechanical Engineering, 42, 393–403, https://doi.org/10.1139/tcsme-2017-0137, 2018.

Reeves, R. and Griffith, D. T.: Intracycle RPM Control for Vertical Axis Wind Turbines: Impacts on System Design and Costs, in: AIAA SCITECH 2025 Forum, American Institute of Aeronautics and Astronautics, https://doi.org/10.2514/6.2025-0648, 2025.

Rezaeiha, A., Kalkman, I., and Blocken, B.: Effect of pitch angle on power performance and aerodynamics of a vertical axis wind turbine, Applied Energy, 197, 132–150, https://doi.org/10.1016/j.apenergy.2017.03.128, 2017.

Ribeiro, A. F. P., Ferreira, C. S., and Casalino, D.: Vertical axis wind turbine wake steering by pitched struts and blades, Journal of Physics: Conference Series, 2767, 092 004, https://doi.org/10.1088/1742-6596/2767/9/092004, 2024.

Rodrigues, O.: Des lois géométriques qui régissent les déplacements d'un système solide dans l'espace, et des variations des coordonnées provenant de ces déplacements considérés indépendamment des causes qui peuvent les produire, Journal de Mathématiques Pures et Appliquées, 5, 380–440, 1840.

Sadman Sakib, M., Todd Griffith, D., Hossain, S., Bayat, S., and Allison, J. T.: Intracycle RPM control for vertical axis wind turbines, Wind Energy, 27, 202–224, https://doi.org/10.1002/we.2885, 2023.

Sakib, M. S. and Griffith, D. T.: Parked and operating load analysis in the aerodynamic design of multi-megawatt-scale floating vertical-axis wind turbines, Wind Energy Science, 7, 677–696, https://doi.org/10.5194/wes-7-677-2022, 2022.

Thomsen, K.: The statistical variation of wind turbine fatigue loads, Tech. Rep. 1063(EN), ISBN 87-550-2410-6, 1998.

Zereg, A., Aksas, M., Bouzaher, M. T., Laghrouche, S., and Lebaal, N.: Efficiency Improvement of Darrieus Wind Turbine Using Oscillating Gurney Flap, Fluids, 9, 150, https://doi.org/10.3390/fluids9070150, 2024.